ISSN 0020-1685, Inorganic Materials, 2015, Vol. 51, No. 11, pp. 1132–1137. © Pleiades Publishing, Ltd., 2015.
Original Russian Text © A.A. Valeeva, K.A. Petrovykh, H. Schroettner, A.A. Rempel, 2015, published in Neorganicheskie Materialy, 2015, Vol. 51, No. 11, pp. 1221–1227.

Effect of Stoichiometry on the Size of Titanium Monoxide Nanoparticles Produced by Fragmentation

A. A. Valeeva[a, b], K. A. Petrovykh[a, b], H. Schroettner[c], and A. A. Rempel[a, b]

[a] *Institute of Solid State Chemistry, Ural Branch, Russian Academy of Sciences, Pervomaiskaya ul. 91, Yekaterinburg, 620990 Russia*

[b] *Ural Federal University, ul. Mira 19, Yekaterinburg, 620002 Russia*

[c] *Institute for Electron Microscopy and Nanoanalysis, Graz University of Technology, Steyrergasse 17/III, A-8010 Graz, Austria*

e-mail: valeeva@ihim.uran.ru

Received March 23, 2015; in final form, May 21, 2015

Abstract—Coarse disordered and ordered titanium monoxide powders differing in composition—substoichiometric ($TiO_{0.92}$), near-stoichiometric ($TiO_{0.97}$ and $TiO_{0.99}$), and superstoichiometric ($TiO_{1.23}$)—have been disintegrated by milling. According to X-ray diffraction and scanning electron microscopy data, milling produced nanoparticles down to 20 ± 10 nm in size. The basic structure of the nanoparticles prepared from the disordered powders was identical to the parent basic structure *B*1. The structure of the nanoparticles prepared from the ordered powders with the *C*2/*m* structure also remained unchanged. Using the Williamson–Hall method, we assessed the effect of the stoichiometry of the starting powder on the size of the nanoparticles and found that an ordered state of near-stoichiometric titanium monoxide ensures a factor of 3 lower lattice strain in the nanoparticles.

DOI: 10.1134/S0020168515110138

INTRODUCTION

The Ti–O system is of both scientific and technological interest because it contains a wide range of compounds of various stoichiometries. The physical and chemical properties of the compounds in the Ti–O system depend not only on their chemical composition and crystal structure but also on the particle size. Titanium dioxide is used in renewable energy sources (solar cells and photoelectrochemical water decomposition) or as a photocatalyst for organic contamination removal [1–10]. Stoichiometric titanium dioxide, TiO_2, has a wide band gap (3.1 to 3.3 eV), independent of its structure. As a result, solar light is only absorbed in the ultraviolet spectral region, whereas visible solar light is either transmitted or reflected [11–13].

To obtain a photocatalyst effective in the visible range, an approach has recently been developed that takes advantage of the decrease in band gap with increasing structural oxygen vacancy concentration [2]. In connection with this, there is currently great practical interest in the preparation and characterization of titanium monoxide nanoparticles, which may contain up to 30 at % oxygen vacancies.

The preparation of nanocrystalline nonstoichiometric titanium monoxide has not received attention previously, even though such materials have properties of practical importance, which may considerably extend their application area not only in catalysis but also in nanoelectronics. For example, titanium oxide nanoparticles were used to produce a single-electron transistor [14]. Such components of electronic circuits employing quantum tunneling effects are used to miniaturize electronic processors and memory systems. Monoxides are also used to grow semiconductor films in optics as antireflection materials. To this end, titanium monoxide is deposited onto a silica substrate and oxidized to titanium dioxide [10].

The objectives of this work were to prepare nanocrystalline titanium monoxide of various compositions through disintegration in a planetary ball mill and assess the effect of titanium monoxide stoichiometry on the size and structural characteristics of the nanoparticles.

EXPERIMENTAL

TiO_y titanium monoxide powders were synthesized by a procedure described in detail elsewhere [15]. The process was run at a temperature of 1773 K in a vacuum of 1.3 mPa for 20 h, followed by homogenization by annealing under the same conditions for 50 h with intermediate grindings. The resultant samples were characterized by determining their chemical and phase compositions, their crystal structure, and the degree of atomic vacancy order.

The preparation of nanoparticles through disintegration is a dispersion method, or a top-down method. Disintegration requires high energy density, which can be reached in planetary ball mills. High-energy

mechanical grinding is a simple, effective, high-performance process for the preparation of various nanocrystalline powders with an average particle size under 100 nm in mills. All other factors being equal, the particle size after milling is smaller at a higher deposited energy, longer milling time, and smaller initial weight and size of the particles. Not only does milling reduce the particle size but it also produces lattice strain in the nanoparticles. As a result, some of the milling energy is consumed to produce lattice strain, which considerably reduces the disintegration rate.

In this study, macrocrystalline titanium monoxide powders of various compositions were disintegrated by high-energy milling in a Retsch PM 200 planetary ball mill. The grinding media and the inner wall of the grinding vials were of Y_2O_3-stabilized ZrO_2, a very hard, high-strength material. The ball-to-powder weight ratio in our experiments was 10 : 1. According X-ray diffraction data, after milling the powders were contaminated with 0.6 wt % yttria-stabilized zirconia. The milling liquid used was isopropanol, $CH_3CH(OH)CH_3$. Nanopowders were produced under the following milling conditions: milling time of 15, 30, 60, 120, 240, and 480 min; rotation direction reversed every 15 min; interval between direction reversals, 5 s; rotation speed of the disk supporting the grinding vials, 500 rpm.

The as-prepared and milled titanium monoxide powders were characterized by X-ray diffraction on a Shimadzu XRD-7000 automatic diffractometer ($CuK_{\alpha_{1,2}}$ radiation). X-ray diffraction patterns were collected in step-scan mode with a step $\Delta(2\theta) = 0.02°$ in the angular range $2\theta = 10°$ to 140° with high statistics.

Diffraction line profiles were analyzed by fitting with pseudo-Voigt functions of the form

$$V(\theta) = ca\left[1 + \frac{(\theta - \theta_0)^2}{\theta_L^2}\right]^{-1} + (1-c)a\exp\left[-\frac{(\theta - \theta_0)^2}{2\theta_G^2}\right], \quad (1)$$

where c is the relative contribution of the Lorentzian to the total intensity of the reflection; θ_L and θ_G are parameters of the Lorentzian and Gaussian functions, respectively; a is an intensity normalizing factor; and θ_0 is the peak position of the function and reflection.

Numerical analysis of X-ray diffraction patterns by a procedure reported elsewhere [16, 17] showed that the powders were homogeneous and single-phase. In connection with this, the average crystallite size was determined as [18, 19]

$$D = K_{hkl}\lambda/\cos\theta\beta(2\theta) \equiv K_{hkl}\frac{\lambda}{2}\cos\theta\beta(\theta), \quad (2)$$

were K_{hkl} is the James coefficient and $\beta(2\theta)$ is broadening. The broadening $\beta(2\theta) \equiv 2\beta(\theta)$ of diffraction peaks was evaluated as

$$\beta(2\theta) = \sqrt{FWHM_{obs}^2 - FWHM_R^2}. \quad (3)$$

The instrumental broadening (the resolution function of the diffractometer) was determined in a special diffraction experiment using a lanthanum hexaboride, LaB_6, powder standard (NIST Standard Reference Powder 660a) with a cubic lattice parameter a_{cubic} = 415.69 pm and a particle size near 10 μm. The resolution function of the diffractometer, determined with lanthanum hexaboride, had the following parameters: $u = 0.0058$, $v = -0.0046$, and $w = 0.0101$.

The particle size and strain contributions to diffraction line broadening were evaluated by the Williamson–Hall method [20, 21]. The reduced width was determined as

$$\beta^*(2\theta) = \beta(2\theta)\cos\theta/\lambda. \quad (4)$$

The observed broadening $\beta(2\theta)$ was contributed by both size (β_s) and strain (β_d) broadening:

$$\beta = \sqrt{\beta_s^2 + \beta_d^2}. \quad (5)$$

The size of a single-crystal nanoparticle can be treated as the crystallite size. In this study, the crystallite size was evaluated as

$$Dcr = 1/\beta^*(2\theta = 0). \quad (6)$$

The crystallite size was determined by extrapolating $\beta^*(s)$ to $s = 0$, and the lattice strain was found from the slope of the resultant straight line. Lattice strain $\varepsilon = \Delta d/d_0$, where d_0 is the average interplanar spacing and Δd is its deviation, leads to a strain-induced diffraction line broadening $\beta_d(2\theta) = 2\varepsilon\tan\theta$.

The microstructure of the as-prepared and ball-milled powders was examined by high-resolution scanning electron microscopy (SEM) with a Zeiss Ultra 55 instrument. The lens–sample distance was 3.9–4.3 mm, the accelerating voltage was 3–5 keV, and the beam width was 2 to 6 μm, depending on magnification. High-resolution SEM measurements led to severe powder charging, which made it impossible to obtain quality images. To prevent specimen surface charging during electron microscopic examination, the powder to be studied was applied to conductive adhesive tape and then covered with a thin chromium layer. The chromium nanolayer was 2 to 4 nm thick, so the chromium coating had no effect on powder morphology visualization quality.

RESULTS AND DISCUSSION

We milled six powders differing in composition and long-range order: substoichiometric disordered titanium monoxide $TiO_{0.92q}$; near-stoichiometric disordered and ordered $TiO_{0.97q}$, $TiO_{0.97a}$, $TiO_{0.99q}$, and $TiO_{0.99a}$; and superstoichiometric disordered $TiO_{1.23q}$ (q and a refer to quenched and annealed samples, respectively). After milling, all of the reflections in the X-ray diffraction patterns of the titanium monoxide samples were markedly broadened.

Figure 1 shows the 220 reflection in the X-ray diffraction pattern of the $TiO_{0.99q}$ unmilled powder

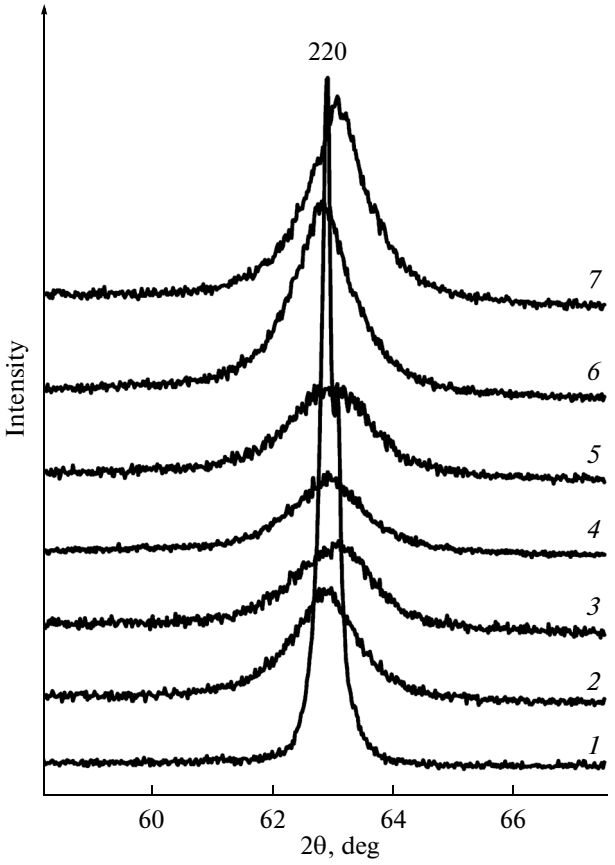

Fig. 1. Broadening of a reflection from (*1*) the unmilled $TiO_{0.99q}$ powder and (*2*–*7*) after milling for 480 min: (*2*) $TiO_{0.99q}$, (*3*) $TiO_{0.99a}$, (*4*) $TiO_{0.97q}$, (*5*) $TiO_{0.97a}$, (*6*) $TiO_{0.92q}$, and (*7*) $TiO_{1.23q}$.

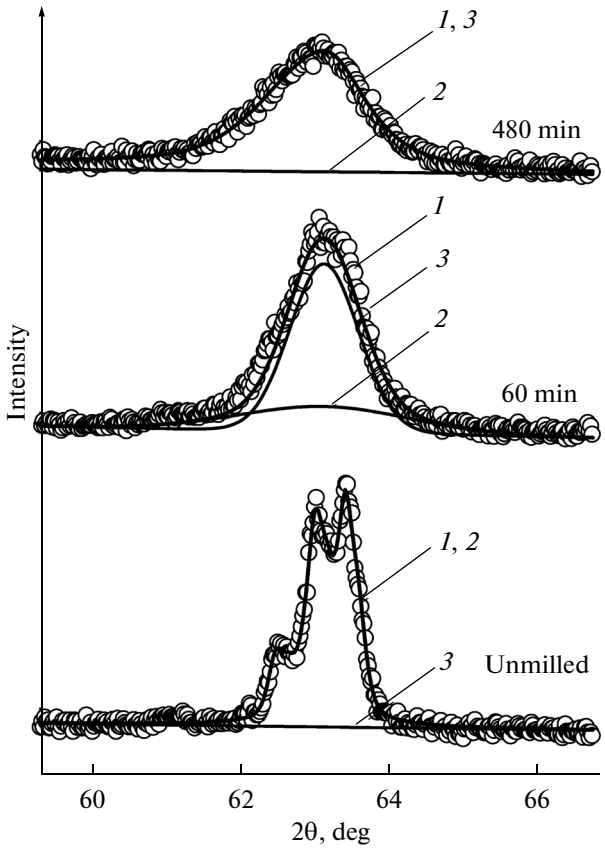

Fig. 2. Fitting of diffraction line profiles of $TiO_{0.99a}$ powders with pseudo-Voigt functions at different milling times: (*1*) sum function, (*2*) contribution of the large particles to the intensity of the reflection, (*3*) contribution of the nanoparticles to the intensity of the reflection.

(scan *1*) and after milling for 480 min for the six powders (scans *2*–*7*). In the diffraction pattern of the unmilled powder, the reflections from the crystalline phase are narrow, and the $\alpha_{1,2}$ doublet splitting is well seen, pointing to high homogeneity of the unmilled powder. Milling reduces the intensity of the reflections and drastically increases their width. The shape of the reflections after milling is almost symmetric, and there is no $\alpha_{1,2}$ doublet splitting.

The broadening of reflections from nanopowders may be caused by breakdown of the translational symmetry and some point group symmetry elements of the parent crystal structure because of the small particle size and also by the lattice strain produced by high-energy milling. Analysis of X-ray diffraction data indicates that the crystal structure of the nanopowder is identical to that of the macrocrystalline powder, which leads us to conclude that the structure of titanium monoxide is very stable to high-energy milling.

Full-profile analysis of X-ray diffraction line profiles showed that broadening of reflections was observed even after milling for just 15 min, but this time was too short for all coarse particles to be uniformly disintegrated, and the milled powders still contained large particles. For this reason, to separate the contributions of the large and small particles, all of the diffraction line profiles were fitted with a combination of four pseudo-Voigt functions. Two pseudo-Voigt functions represented reflections from the large particles, and two, from the nanoparticles.

Figure 2 illustrates the effect of milling time on the partial contribution of $TiO_{0.99a}$ particles of various sizes to the intensity of the 220 reflection. It is seen that, in the case of the unmilled, coarse powder, the contribution of nanoparticles to the intensity of the reflection is zero. After 60 min of milling, the partial contribution of the nanoparticles to the intensity of the reflection increases to 60%. After milling for 480 min, it reaches 100%. According to the data in Fig. 3, the percentage of the large particles rapidly decreases with increasing milling time. After 240 min of milling, no large particles can be detected in the powder. Also shown in Fig. 3 is the average crystallite size D_{cr} as a function of milling time τ for the $TiO_{0.99a}$ titanium monoxide powder. The experimental data are well represented by the hyperbolic function [22]

$$D(\tau) = (D_0 - D_{min})/(1 + b\tau) + D_{min}, \quad (7)$$

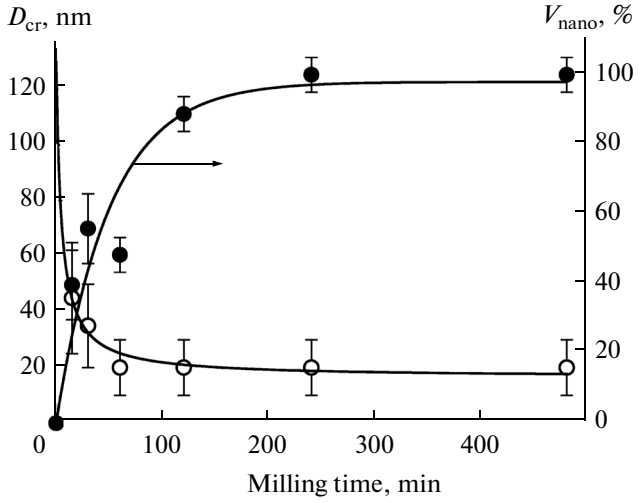

Fig. 3. Crystallite size (D_{cr}) and volume fraction of nanoparticles (V_{nano}) as functions of milling time for the $TiO_{0.99a}$ powder.

where D_0 is the initial particle size (before milling); D_{min} is the minimum particle size that can be reached by milling; and b is a coefficient related to the softness and brittleness of the material, which characterizes the disintegration rate, that is, how rapidly one can disintegrate the material and reach the minimum particle size. The model function parameters obtained in this study demonstrate that, in the case of titanium monoxide, the minimum particle size that can be reached by milling approaches $D_{min} = 20 \pm 10$ nm.

Figure 4 shows the crystallite size D_{cr} and lattice strain ε (inset) as functions of y = O/Ti (the open and filled data points correspond to the disordered and ordered powders, respectively). Analysis of the effect of milling time on the particle size of the substoichiometric ($TiO_{0.92}$), near-stoichiometric ($TiO_{0.97}$ and $TiO_{0.99}$), and superstoichiometric ($TiO_{1.23}$) samples indicates that the crystallite size of the titanium monoxide powders milled for 480 min decreases from 550 to 40 ± 10 nm in the disordered titanium monoxides and to 20 ± 10 nm in the ordered powders.

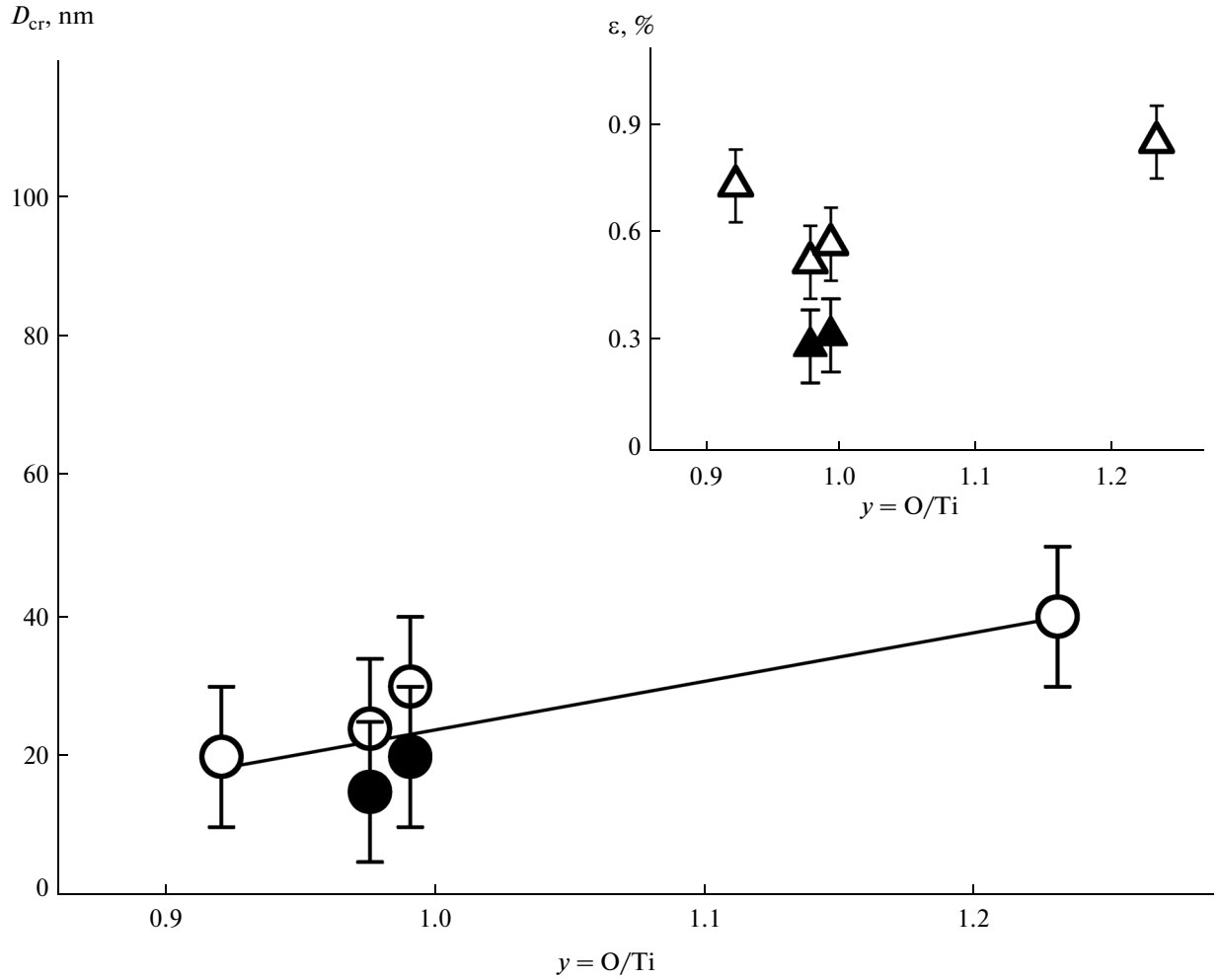

Fig. 4. Crystallite size D_{cr} and lattice strain ε (inset) as functions of y = O/Ti. The open and filled data points correspond to the disordered and ordered samples, respectively.

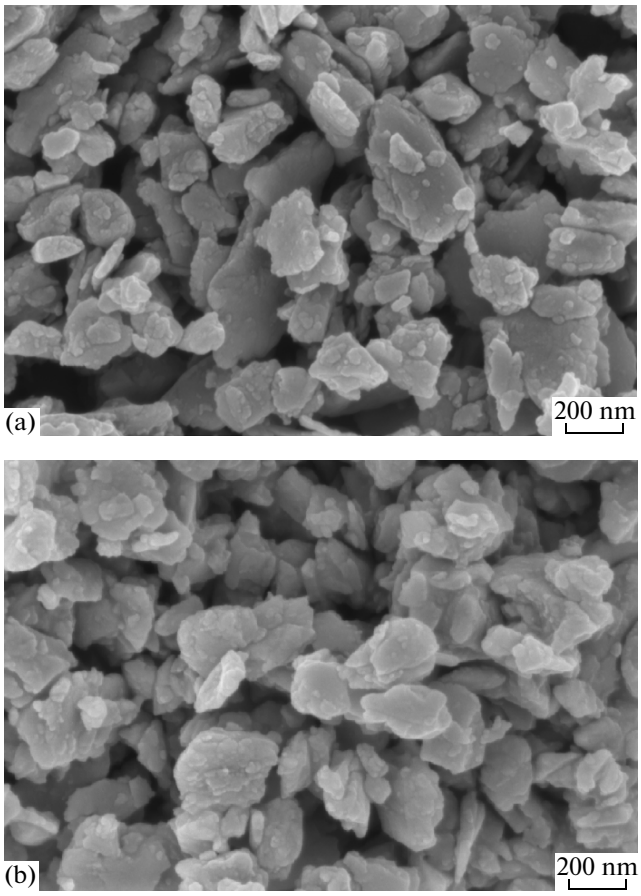

Fig. 5. High-resolution SEM images of (a) disordered titanium monoxide and (b) ordered titanium monoxide powders after milling for 8 h: dense polycrystals consisting of a large number of nanoparticles about 20 nm in size.

D_{cr} as a function of y is well represented by the linear function $D(y) = -45.43 + 69.34y$. In the ordered titanium monoxides milled for 480 min, the minimum particle size, 20 ± 10 nm, is reached, and ε is a factor of 3 lower than the lattice strain in the disordered samples.

Figure 5 shows micrographs of the $TiO_{0.97q}$ disordered and $TiO_{0.97a}$ ordered titanium monoxide powders after milling for 480 min. It is seen from the micrographs that the particles have a rounded shape and range in size from 20 to 30 nm. The nanoparticles stick to each other to form dense polycrystals ranging in size from 40 to 300 nm. Thus, the large particles observed in SEM micrographs consist of many small single-crystal nanoparticles.

CONCLUSIONS

Titanium monoxide powders differing in composition and structural order, with average crystallite sizes from 20 to 40 nm, have been prepared by disintegrating coarse powders. The nanoparticle size depends on the composition of the titanium monoxide: the lower the oxygen content of the monoxide, the smaller the nanoparticle size. By milling ordered near-stoichiometric titanium monoxides, one can obtain nanoparticles 20 ± 10 nm in size. Such nanoparticles suffer the lowest lattice strain: about 0.3%. Milling disordered titanium monoxides, both sub- and superstoichiometric, produces a factor of 3 higher lattice strain.

ACKNOWLEDGMENTS

This research was supported by the Russian Science Foundation (project no. 14-23-00025) and performed at the Institute of Solid State Chemistry, Ural Branch, Russian Academy of Sciences.

REFERENCES

1. Ananikov, V.P., Khemchyan, L.L., Ivanova, Yu.V., Bukhtiyarov, V.I., Sorokin, A.M., Prosvirin, I.P., Vatsadze, S.Z., Medved'ko, A.V., Nuriev, V.N., Dil'man, A.D., Levin, V.V., Koptyug, I.V., Kovtunov, K.V., Zhivonitko, V.V., Likholobov, V.A., et al., Advances in the methodology of modern selective organic synthesis: atomically accurate engineering of functionalized molecules, *Usp. Khim.*, 2014, vol. 83, no. 10, pp. 885–985.
2. Rempel, A.A., Sulfide-, carbide-, and oxide-based hybrid nanoparticles, *Izv. Akad. Nauk, Ser. Fiz.*, 2013, no. 4, pp. 857–869.
3. Rempel, A.A., Nanotechnologies, properties, and applications of nanostructured materials, *Usp. Khim.*, 2007, vol. 76, no. 5, pp. 474–500.
4. Varghese, O.K., Paulose, M., LaTempa, T.J., and Craig, A., High-rate solar photocatalytic conversion of CO_2 and water vapor to hydrocarbon fuels, *Nano Lett.*, 2009, vol. 9, no. 2, pp. 731–737.
5. Hermann, J.M., Duchamp, C., Karkmaz, M., Bui Thu Hoai, Lachheb, H., Puzenat, E., and Guillard, C., Environmental green chemistry as defined by photocatalysis, *J. Hazard. Mater.*, 2007, vol. 146, no. 3, pp. 624–629.
6. O'Regan, B. and Gratzel, M., A low-cost, high-efficiency solar cell based on dye-sensitized colloidal TiO_2 films, *Nature*, 1991, vol. 353, pp. 737–740.
7. Gratzel, M., Photoelectrochemical cells, *Nature*, 2001, vol. 414, pp. 338–344.
8. Fujishama, A. and Honda, K., Electrochemical photolysis of water at a semiconductor electrode, *Nature*, 1972, vol. 298, pp. 37–38.
9. Akikusa, J. and Khan, S.U.M., Photoelectrolysis of water to hydrogen in *p*-SiC/Pt and *p*-SiC/*n*-TiO_2 cells, *Int. J. Hydrogen Energy*, 2002, vol. 27, no. 9, pp. 863–870.
10. Seo, S.G., Park, C-H., Kim, H-Y., Nam, W.H., Jeong, M., Choi, Y-N., Lim, Y-S., Seo, W.-S., Kim, S.-J., Lee, J-Y., and Cho, Y-S., Preparation and visible-light photocatalysis of hollow rock-salt $TiO_{1-x}N_x$ nanoparticles, *J. Mater. Chem. A*, 2013, vol. 1, pp. 3639–3644.

11. Chen, X. and Mao, S.S., Titanium dioxide nanomaterials: synthesis, properties, modifications, and applications, *Chem. Rev.*, 2007, vol. 107, no. 7, pp. 2891–2959.
12. Simon, P., Pignon, B., Miao, B., Coste-Leconte, S., Leconte, Y., Marguet, S., Jegou, P., Bouchet-Fabrie, B., Reynaud, C., and Herlin-Boime, N., N-doped titanium monoxide nanoparticles with TiO rock-salt structure, low-energy band gap, and visible light activity, *Chem. Mater.*, 2010, vol. 22, no. 12, pp. 3704–3711.
13. Chen, X., Liu, L., Yu, P.Y., and Mao, S.S., Increasing solar absorption for photocatalysis with black hydrogenated titanium dioxide nanocrystals, *Science*, 2011, vol. 331, no. 6018, pp. 746–750.
14. Schöllmann, V., Johansson, J., Andersen, K., and Haviland, D.B., Coulomb blockade effects in anodically oxidized titanium wires, *J. Appl. Phys.*, 2000, vol. 88, no. 11, pp. 6549–6553.|
15. Valeeva, A.A., Rempel', A.A., and Gusev, A.I., Ordering of cubic titanium monoxide into monoclinic Ti_5O_5, *Inorg. Mater.*, 2001, vol. 37, no. 6, pp. 603–612.
16. Rempel', A.A., Rempel', S.V., and Gusev, A.I., Quantitative assessment of homogeneity of nonstoichiometric compounds, *Dokl. Phys. Chem.*, 1999, vol. 369, nos. 4–6, p. 321.
17. Rempel, A.A. and Gusev, A.I., Preparation of disordered and ordered highly nonstoichiometric carbides and evaluation of their homogeneity, *Phys. Solid State*, 2000, vol. 42, no. 7, pp. 1280–1286.
18. Warren, B.E., *X-ray diffraction*, New York: Dover, 1990.
19. James, R.W., *The Optical Principles of the Diffraction of X-Rays*, London: Bell, 1950.
20. Hall, W.H., X-ray line broadening in metals, *Proc. Phys. Soc. London: Sect. A*, 1949, vol. 62, part 11, no. 359, pp. 741–743.
21. Hall, W.H. and Williamson, G.K., The diffraction pattern of cold worked metals: I. The nature of extinction, *Proc. Phys. Soc. London: Sect. B*, 1951, vol. 64, part 11, no. 383, pp. 937–946.
22. Valeeva, A.A., Schroettner, H., and Rempel, A.A., Disintegration of disordered stoichiometric titanium monoxide, *Izv. Akad. Nauk, Ser. Khim.*, 2014, no. 12, pp. 2729–2732.